Design and study of $BiVO_4/MnCo_2O_4$ nanocomposites for visible light-driven antibacterial applications

K. N. V. Suguna Sarvani[1], Lingayya Hiremath[2] and N. Manikanda Prabu[1,*]

[1]Department of Chemistry, Faculty of Mathematical and Physical Sciences, M.S. Ramaiah University of Applied Sciences, Bengaluru 560 058, India
[2]R.V. College of Engineering, Mysore Road, R.V. Vidyaniketan, Post, Benglauru 560 059, India

In this study, $BiVO_4$ and $MnCo_2O_4$ were synthesized successfully using hydrothermal and co-precipitation methods. Nanocomposites of $BiVO_4/MnCo_2O_4$ of varying composition were made by calcination. All the synthesized compounds were well-characterized using PXRD, SEM, EDS and DRS. Powder XRD analysis confirmed the formation of $BiVO_4$, $MnCo_2O_4$ and their respective well-defined composites. The band gaps of the materials were in the visible range (1.16–2.36 eV), making them suitable for visible light-driven antibacterial applications to inactivate the Gram-negative bacterium *Escherichia coli*. The as-prepared composites exhibited superior antibacterial activity (maximum of ~80%) than the parent compounds, possibly due to the synergistic effect.

Keywords: Antibacterial applications, *Escherichia coli*, nanocomposites, semiconductor, synergistic effect.

INFECTIOUS microorganisms present in waterbodies can spread harmful diseases, so disinfection is inevitable to maintain safety and well-being of the society[1]. The need for clean water demands effective disinfection methods and agents. The chemical disinfecting agents have certain limitations such as instability, formation of harmful by-products[2,3] and inducing bacterial resistance[4,5]. Hence, non-toxic and potential antibacterial agents are necessary for effective disinfection which can ensure the control of pathogenic microorganisms. Recently, nanomaterials have attracted attention due to their potential antimicrobial properties[6,7]. Semiconducting photocatalytic nanomaterials in particular exhibit appreciable antibacterial activity under light irradiation with immense possibilities to achieve effective disinfection.

Recently, antibacterial properties of many nanomaterials such as TiO_2, $BiVO_4$, Bi_2WO_6 and Bi_2O_3 have been studied[8]. Among them, TiO_2 has been reported to exhibit potential activity under ultraviolet irradiation[9]. However, in the visible region, the activity is not impressive. Thus, there is a need to develop materials which can show potential activity in the visible region. High photocatalytic efficiency can be achieved by various methods such as modification of band structures, doping or heterojunctioning[10]. Heterojunctioning or composite formation can provide potential antibacterial activity to semiconducting nanomaterials towards the inactivation of microorganisms by decreasing their rate of recombination of charges. Also, composites possess many advantages such as stability, recyclability and high efficiency[11,12]. In recent times, monoclinic scheelite $BiVO_4$ has attracted attention due to its ease of preparation, thermal/photochemical stability, tunable band gap and potential antibacterial activity[13,14]. $BiVO_4$ has been analysed for the degradation of organic pollutants, and further research on antibacterial applications can give new insights into this field of study. $MnCo_2O_4$ exhibits thermal/photochemical stability, desired band gap and photocatalytic property[15]. However, only a few studies have been carried out on the antibacterial activities of $MnCo_2O_4$. Nanocomposites of hydrothermally prepared $BiVO_4$ and $MnCo_2O_4$ prepared by the co-precipitation method are yet to be studied for their antibacterial properties. Hence, the present study analyses the preparation of $BiVO_4$ and $MnCo_2O_4$ as well as their composites and their antibacterial properties.

Experimental method

Materials used

$Bi(NO_3)_3{\cdot}5H_2O$ (99.9%) and NH_4VO_3 (99.9%) were purchased as analytical-grade reagents from Sigma-Aldrich, USA. NaOH (99.5%), $MnCl_2{\cdot}4H_2O$ (99.5%) and $CoCl_2{\cdot}6H_2O$ (99.5%) were purchased from SD Fine-Chem. Ltd, India. For culture growth, Luria–Bertani (LB) broth (Accumix-India) and for the preparation of Petri plates, agar-agar type-I (HIMEDIA-India) were used. *Escherichia coli* culture was used from ATCC bacterial cultures (Sigma-Aldrich). For the colony count method, solid medium agar plates were prepared from LB media and 2% agar powder (Accumix-India and HIMEDIA-India). All solutions were prepared in double-distilled water.

Preparation of $BiVO_4$, $MnCo_2O_4$ and $BiVO_4/MnCo_2O_4$ composites

$Bi(NO_3)_3{\cdot}5H_2O$ and NH_4VO_3 were taken in stoichiometric amounts and employing the hydrothermal method $BiVO_4$

*For correspondence. (e-mail: manikanda.cy.mp@msruas.ac.in)

was prepared as reported elsewhere[16]. $MnCl_2·4H_2O$ and $CoCl_2·6H_2O$ were taken along with NaOH and ascorbic acid to prepare $MnCo_2O_4$ as explained elsewhere[17]. Three different composites were prepared by calcining the mixtures of $BiVO_4$ and $MnCo_2O_4$ (sample codes: $BiVO_4$–BVO; $MnCo_2O_4$–MCO; 25 wt% $BiVO_4$ + 75 wt% $MnCo_2O_4$ – composite 1; 50 wt% $BiVO_4$ + 50 wt% $MnCo_2O_4$ – composite 2; 75 wt% $BiVO_4$ + 25 wt% $MnCo_2O_4$ – composite 3).

The detailed procedure is discussed in the Supplementary Material.

Characterization techniques

Powder X-ray diffraction (XRD) patterns were recorded using PANalytical X-ray diffractometer equipped with Cu-Kα radiation. Scanning electron microscopy (SEM) studies were carried out (Tescan-Mira 3 LMH) and the compounds were analysed using energy-dispersive X-ray spectroscopy (EDS; Bruker Quantax 200). Diffuse reflectance spectra (DRS) were recorded using a spectrophotometer (Shimadzu UV-260).

Antibacterial studies

Bacterial medium preparation and culture growth: All glassware were autoclaved for 15 min at 121°C at 15 psi pressure. Standard *E. coli* culture (ATCC bacterial cultures, Sigma-Aldrich) was used for growth. Luria broth (LB) solution of 250 ml was prepared and 1 ml of standard *E. coli* was added. The culture was grown overnight in a bacteriological incubator at 37°C. It was then centrifuged at 3500 rpm for 15 min, separated from the medium and resuspended in 250 ml of sterile deionized water. The antibacterial activity was analysed using the standard colony count method. For all the antibacterial studies, the solutions were prepared identically by taking 100 μl of bacterial solution and making it up to 100 ml in volume with saline solution (dilution factor = 10^{-3}). The initial cell concentration was adjusted to be 1×10^7 colony forming units (CFUs)/ml for all the experiments[18,19]. For each experiment, 100 ml of bacterial solution was taken and a known amount of the compound (0.05 g/100 ml) was added and stirred for 1 min. This mixture was used for antibacterial studies under visible light irradiation in a homemade reactor, the details of which are explained elsewhere[11].

Colony count analysis: For colony count analysis, solid medium agar plates were prepared from LB medium and 2% agar powder solution. For analysis, 10 μl of the reacted sample (without serial dilution) was collected at regular intervals and spread on the agar plate using a sterile glass rod. The plates for different time intervals (0, 30, 60, 90 and 120 min) were incubated overnight and visible colonies were counted. The viable cells on each plate at different time intervals were plotted as a function of time. Equations (1) and (2) were used to calculate CFUs/ml and dilution factor[20,21].

$$\text{Colony forming units/ml} = \frac{\text{Number of colonies} \times \text{dilution factor}}{\text{Volume of sample taken on petri plate}}. \quad (1)$$

$$\text{Dilution factor} = \frac{\text{Volume of stock solution taken}}{\text{Total volume (stock + diluent)}}. \quad (2)$$

Results and discussion

Powder XRD analysis

Figure 1 shows the powder XRD patterns of $BiVO_4$, $MnCo_2O_4$ and three composites. The formation of monoclinic scheelite $BiVO_4$ was confirmed from the powder XRD pattern. The characteristic peaks (19°, 28.8°, 30.5°, 34.5°, 35.1°, 39.8°, 42.5°, 46°, 46.7°, 47.4°, 50.0°, 53.3°, 58.4° and 59.6°) of monoclinic $BiVO_4$ were observed and matched well with the JCPDS file no. 14–688 having space group I2/a (ref. 16). However, the hydrothermally prepared compound contained a small amount of tetragonal $BiVO_4$ as a secondary phase, which was evident from the observed characteristic peaks of the tetragonal phase at 24.4° and 32.7° (ref. 22). Formation of $MnCo_2O_4$ by co-precipitation was confirmed from the characteristic peaks of the phase at 18.9°, 31.2°, 36.8°, 38.4°, 44.6°, 55.5°, 59.1° and 65.1°. The observed peaks matched with the JCPDS file no. 23-1237 having a space group fd3m (ref. 17). The powder XRD patterns of the composites exhibited peaks from both $BiVO_4$ and $MnCo_2O_4$

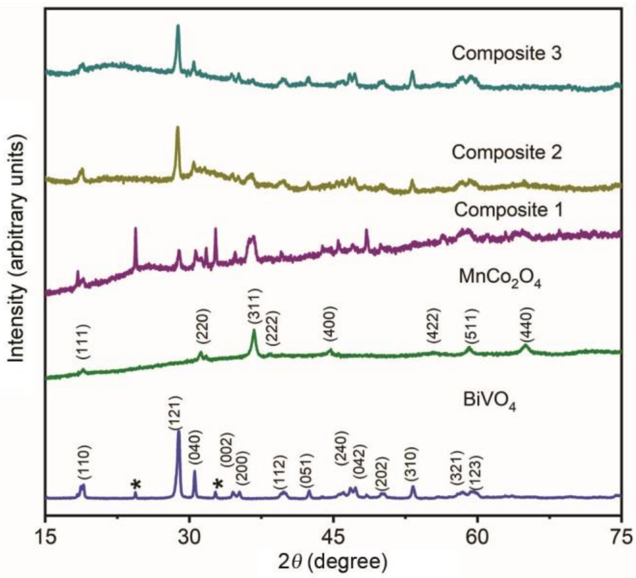

Figure 1. Powder XRD patterns of as-prepared $BiVO_4$, $MnCo_2O_4$ and their composites (* indicates peaks from secondary tetragonal $BiVO_4$ phase).

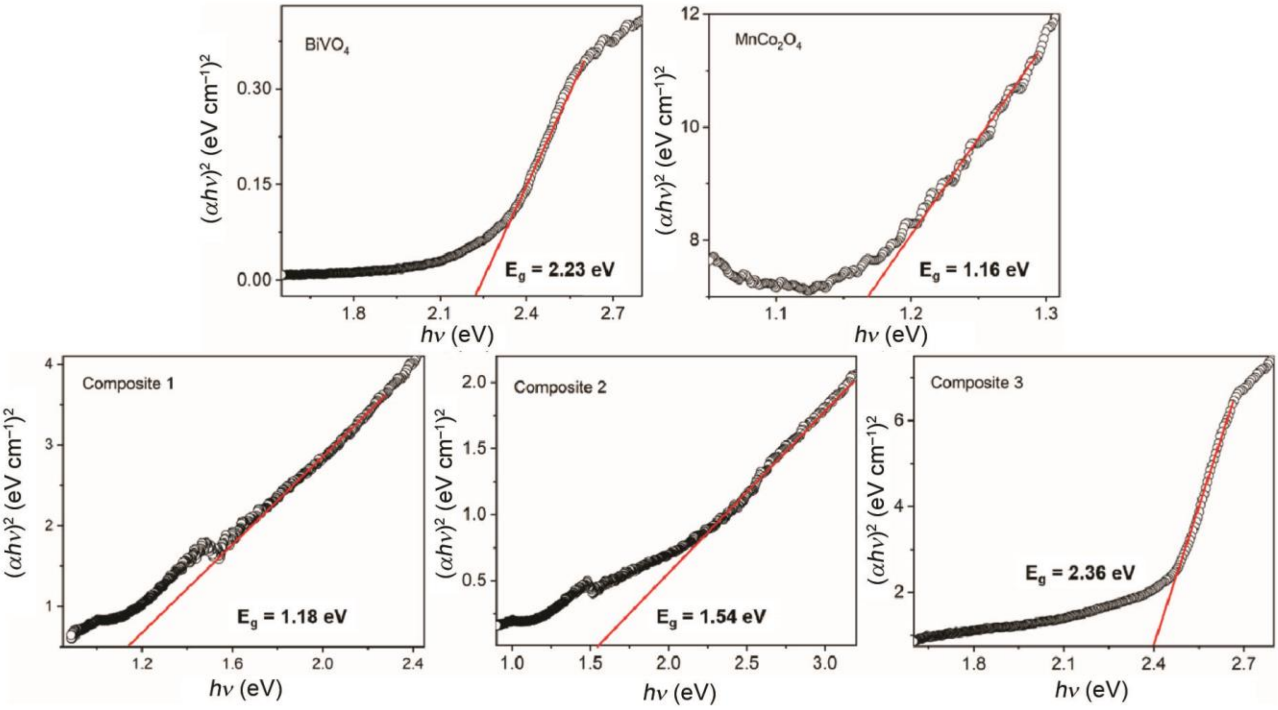

Figure 2. Tauc plots to determine band gaps of all the as-prepared compounds estimated using absorption data from diffuse reflectance spectra.

phases. The intensity of the peaks corresponding to $BiVO_4$ phase increased from composite 1 to composite 3 as the $BiVO_4$ content increases in the overall composition. Similarly, the intensity of peaks corresponding to $MnCo_2O_4$ phase decreased from composite 1 to composite 3 as the $MnCo_2O_4$ content decreased in the overall composition. This observation confirms the formation of well-defined composites between the two phases. The peaks of the secondary tetragonal $BiVO_4$ phase were more intense in composite 1, but suppressed in composites 2 and 3. This indicates the presence of a relatively more monoclinic $BiVO_4$ phase than the tetragonal $BiVO_4$ phase in composites 2 and 3.

Band-gap studies

Band gaps of all the as-prepared compounds were estimated by Tauc plots using the absorbance data obtained from diffuse reflectance spectra (Figure 2). Hydrothermally prepared $BiVO_4$ exhibited a band gap of 2.23 eV, which was comparable to the values reported in the literature[23,24]. $MnCo_2O_4$ prepared using the co-precipitation method exhibited a band gap of 1.16 eV and that both band-gap values were within the visible region. Composite 1, composite 2 and composite 3 showed band gaps of 1.18, 1.54 and 2.36 eV respectively. The band-gap values of the composites increased as the $BiVO_4$ phase increased or the $MnCo_2O_4$ phase decreased in the overall composition. This observation confirms the formation of well-defined composites between the $BiVO_4$ and $MnCo_2O_4$ phases. Since these composites exhibit band gaps in the visible region, this study further examined their applications under visible light irradiation.

Morphology and elemental analysis

Morphology of all the as-prepared powders was studied using SEM (Figure 3). The samples consisted of spherical, irregular and elongated plate-like particles. The average particle size of $BiVO_4$ was 148 nm (ref. 11) and relatively larger than the $MnCo_2O_4$ particles and the composites. The average particle size of $MnCo_2O_4$ was found to be 83 nm. Both large and small particles were visible in composite 1, composite 2 and composite 3 with average particle sizes of 85, 99 and 125 nm respectively. Apart from the smaller and slightly larger particles, an agglomeration of particles was also observed leading to larger aggregations in $MnCo_2O_4$ and the composites. As the content of $BiVO_4$ phase increased in the composites, the average particle size also increased. Elemental analysis of all the compounds was done using their EDS spectra by choosing random spots on each of the as-prepared powder samples. The respective elements were observed in the EDS spectra and the compounds were found to be free from any impurities from the container (alumina) material. The corresponding EDS spectra of all samples are shown in Supplementary Figure 1.

Antibacterial studies

Antibacterial studies were performed on the Gram-negative bacteria *E. coli* (100 ml bacterial solution) with an initial

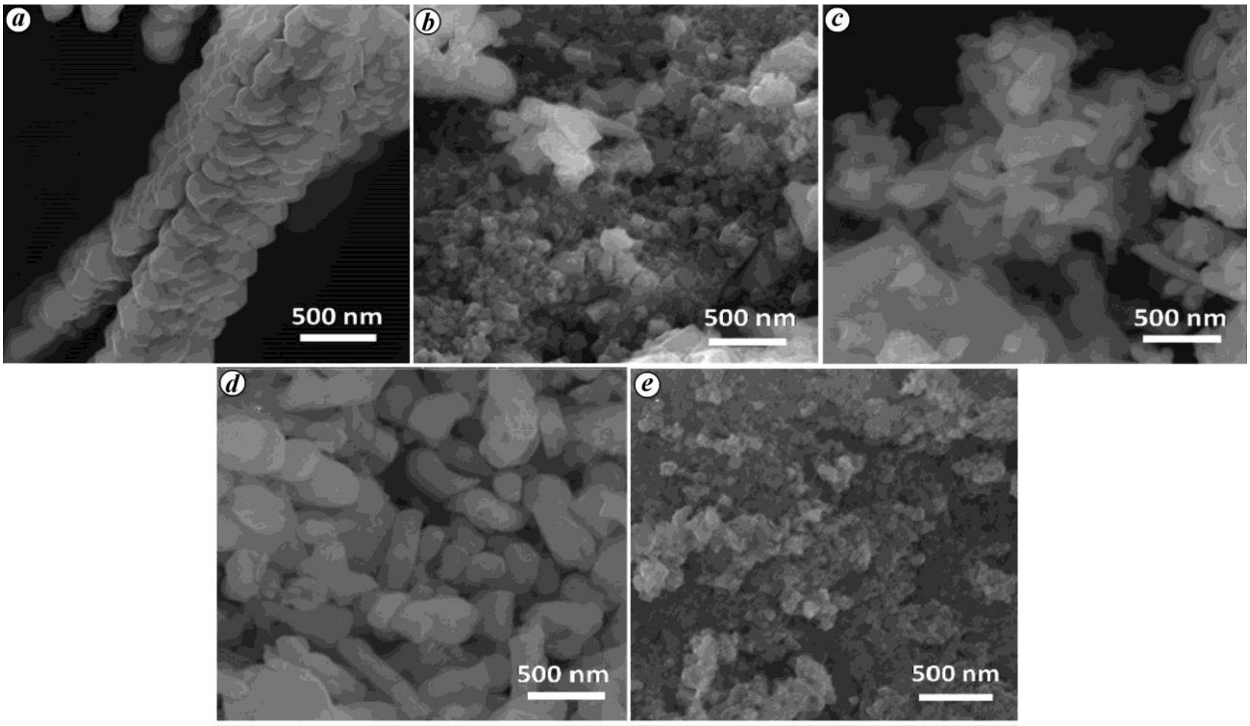

Figure 3. SEM images of as-prepared $BiVO_4$, $MnCo_2O_4$ and their composites. (***a***) $BiVO_4$, (***b***) composite 1, (***c***) composite 2, (***d***) composite 3 and (***e***) $MnCo_2O_4$.

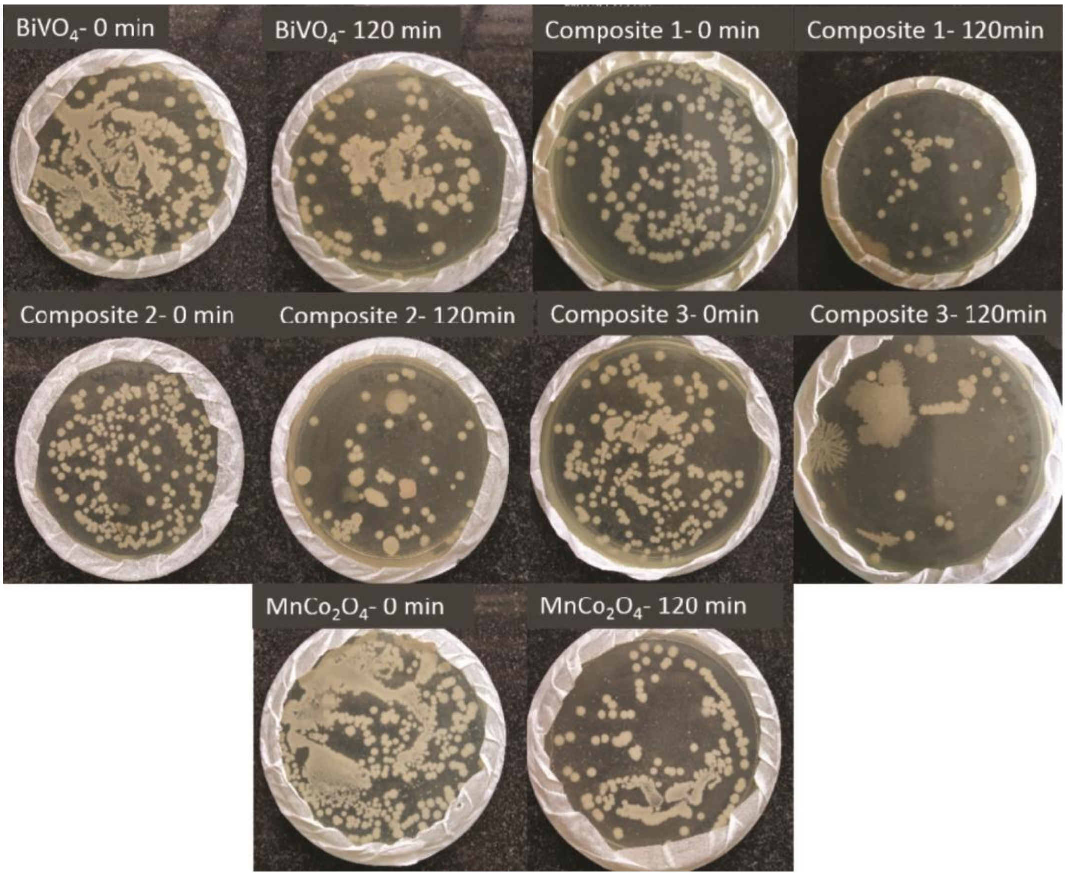

Figure 4. Images of bacterial colonies before (0 min) and after (120 min) the visible light-driven experiments for the study of antibacterial activity on *Escherichia coli*.

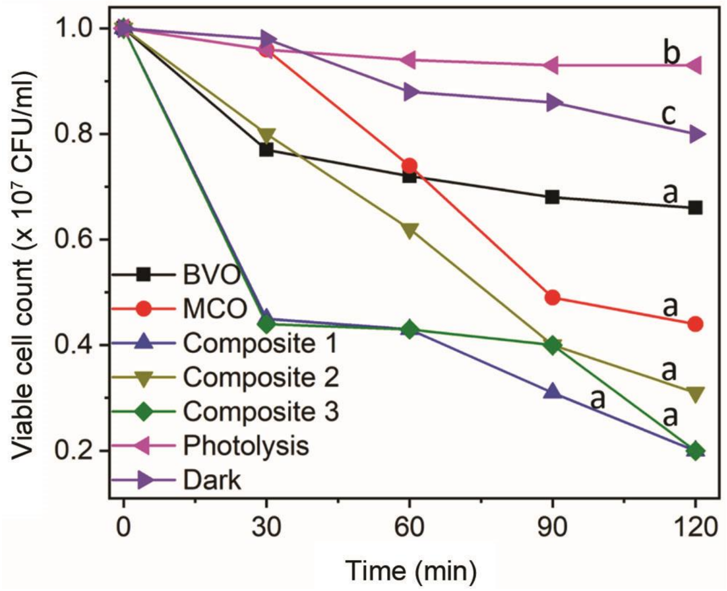

Figure 5. Plot of viable cell count vs time indicating the inactivation of *E. coli* as a function of time: (***a***) as-prepared compounds, (***b***) photolysis (with light and without composite) and (***c***) dark experiment (without light and with composite).

cell concentration of 1×10^7 CFUs/ml for all the as-prepared compounds. The concentration of the compounds was 0.05 g/100 ml for all samples. Figure 4 shows the bacterial colonies before and after antibacterial studies. After counting the colonies at different time intervals using eqs (1) and (2), the viable cells were counted and plotted. Figure 5 shows the viable cell counts as a function of time for *E. coli* under visible-light irradiation for all compounds. The antibacterial activity can be estimated by the decrease in viable cell count, which indicates the inactivation of microorganisms. As shown in Figure 5 *a*, $BiVO_4$ shows ~34% inactivation of *E. coli* in 2 h under visible-light irradiation. $MnCo_2O_4$ shows slightly higher inactivation efficiency under the same conditions, which is ~56%. All three composites exhibit better activity compared to $BiVO_4$ and $MnCo_2O_4$. Composite 2 shows the lowest efficiency in the inactivation, which is ~69% in 2 h. Composites 1 and 3 show the highest and almost similar efficiencies in the inactivation of microorganisms, which is ~80% in 2 h under visible-light irradiation. This indicates that the composites exhibit superior antibacterial properties compared to the individual $BiVO_4$ and $MnCo_2O_4$ compounds due to the synergistic effect of composite formation. Photolysis experiment was performed in order to examine the inactivation of microorganisms by light (with light and without any composite/compound) (Figure 5 *b*). The experiment was also performed in dark conditions (without light and with composite 3 or composite 1) to analyse the efficiency of the composite without light (Figure 5 *c*). Photolysis for 2 h led to ~7% inactivation of *E. coli*. Composite 3 or composite 1 in dark conditions (without light) exhibited ~20% inactivation against *E. coli* in 2 h. Both experiments showed a small decrease in the viable count. Thus it is clear that the composites are effective only in visible light. These findings confirm that composites 1 and 3 are potential antibacterial materials under visible-light irradiation, which can be used for *in vitro* antibacterial applications. The viable cell counts at different time intervals for the experiments under visible-light irradiation and photolysis/dark conditions are given in the Supplementary Tables 1 and 2 respectively.

Based on the results obtained, a possible mechanism is proposed to explain the enhanced visible light-driven antibacterial activity of the composites compared to the parent compounds (Figure 6)[25–27]. Figure 6 explains the transfer of photogenerated charge carriers and the separation of electrons and holes in the composites. The valance and conduction band edge potential of $BiVO_4$ was 1.90 eV and –0.33 eV respectively. Similarly, the valance and conduction band edge potential of $MnCo_2O_4$ was 1.11 and –0.05 eV respectively, which were calculated using the Butler–Ginley equation[28–31]. The electrons were transferred from the conduction band of $BiVO_4$ to the conduction band of $MnCo_2O_4$. Similarly, the holes were transferred from the valance band of $BiVO_4$ to the valence band of $MnCo_2O_4$. Thus, the charges were effectively separated and their recombination became less effective. This led to enhanced activity of the composites towards the inactivation of *E. coli* under visible-light irradiation. Further, the electrons and holes can react with the medium and produce reactive species that can in turn react with the microorganisms and damage them. Hydroxyl radicals, hydrogen peroxide and superoxide radicals are the possible reactive species which can be generated by this process. According to the literature, hydroxyl and superoxide radicals play a crucial role in the

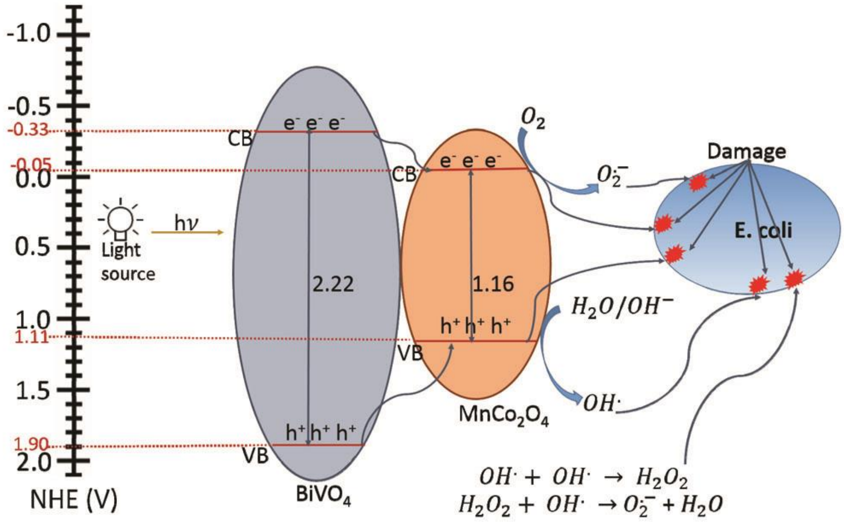

Figure 6. Visible light-induced charge carrier transport and proposed mechanism for the inactivation of *E. coli*[27–32]. NHE, Normal hydrogen electrode.

inactivation process[28–31]. The reactions are explained in eqs (3)–(6). The interaction with these active species and *E. coli* can lead to the following effects such as damage to the cell membrane, interruption of electron transport, DNA damage and oxidation of cell components, which can eventually result in the inactivation of the microorganism[32,33]. Hence, the nanocomposites can effectively inactivate the microorganisms and they can be considered as potential candidates for disinfection in the near future. A detailed comparison of the light-induced photocatalytic activity in the present study and photocatalysts from the literature is given in the Supplementary Table 3.

$$O_2 + e^- \rightarrow O_2^-, \quad (3)$$

$$H_2O/OH^- + h^+ \rightarrow OH^\bullet, \quad (4)$$

$$OH^\bullet + OH^\bullet \rightarrow H_2O_2, \quad (5)$$

$$H_2O_2 + OH^\bullet \rightarrow O_2^{\bullet-} + H_2O. \quad (6)$$

Conclusion

$BiVO_4$, $MnCo_2O_4$ and their respective nanocomposites were successfully synthesized in this study. Powder XRD revealed the formation of well-defined composites of $BiVO_4$ and $MnCo_2O_4$ phases. Average particle size of the composites was close to 100 nm and their size increased as the $BiVO_4$ phase increased in the overall composition. Estimated band gaps of as-prepared compounds were in the visible range and so visible light-driven bacterial inactivation studies were carried out against *E. coli*. Composites 1 and 3 showed the highest inactivation efficiency (~80%) against *E. coli*. Thus, this study showcases promising materials with potential activity for disinfection or antibacterial applications.

Conflict of interest: The authors declare that they have no conflict of interest.

1. McEvoy, J. G. and Zhang, Z., Antimicrobial and photocatalytic disinfection mechanisms in silver-modified photocatalysts under dark and light conditions. *J. Photochem. Photobiol. C*, 2014, **19**, 62–75.
2. Kubacka, A., Ferrer, M., Arias, A. M. and Garcia, M. F., Ag promotion of TiO_2-anatase disinfection capability: study of *Escherichia coli* inactivation. *Appl. Catal. B*, 2008, **84**, 87–93.
3. Sontakke, S., Mohan, C., Modak, J. and Madras, G., Visible light photocatalytic inactivation of *Escherichia coli* with combustion synthesized TiO_2. *Chem. Eng. J.*, 2012, **189–190**, 101–107.
4. Sharma, R. U., Singh, S., Verma, A. and Khanuja, M., Visible light induced bactericidal and photocatalytic activity of hydrothermally synthesized $BiVO_4$ nano-octahedrals. *J. Photochem. Photobiol. B*, 2016, **162**, 266–272.
5. Bushra, R. *et al*., Synthesis, characterization, antimicrobial activity and applications of polyaniline Ti(IV) arsenophosphate adsorbent for the analysis of organic and inorganic pollutants. *J. Hazard. Mater*., 2014, **264**, 481–489.
6. Savage, N. and Diallo, M. S., Nanomaterials and water purification: opportunities and challenges. *J. Nanopart. Res*., 2005, **7**, 331–342.
7. Haas, C. N., Disinfection in the twenty-first century. *J. Am. Water Works Assoc*., 2000, **92**, 72–73.
8. Owonubi, S. J., Malima, N. M. and Revaprasadu, N., Metal oxide based nanocomposites as antimicrobial and biomedical agents. In *Antibiotic Materials in Healthcare* (eds Kokkarachedu, V., Kanikireddy, V. and Sadiku, R.), Academic Press, Cambridge, UK, 2020, pp. 287–323.
9. Raghunath, A. and Perumal, E., Metal oxide nanoparticles as antimicrobial agents: a promise for the future. *Int. J. Antimicrob. Agents*, 2017, **49**, 137–152.
10. Cai, Y. and Feng, Y. P., Review on charge transfer and chemical activity of TiO_2: mechanism and applications. *Prog. Surf. Sci*., 2016, **91**, 183–202.
11. Remlalfaka, W., Murugesan, C., Anantharamaiah, P. N. and Prabu, N. M., Fabrication of magnetically recoverable $BiVO_4/NiFe_2O_4$

composites for the photocatalytic degradation of methylene blue. *Ceram. Int*., 2021, **47**, 11526–11535.
12. Bavani, T., Madhavan, J., Prasad, S., Al Salhi, M. S., AL Jaffreh, M. and Vijayanand, S., Fabrication of novel $AgVO_3$/BiOI nanocomposite photocatalyst with photoelectrochemical activity towards the degradation of rhodamine B under visible light irradiation. *Environ. Res.*, 2021, **200**, 111365.
13. Malathi, A., Madhavan, J., Ashokkumar, M. and Arunachalam, P., A review on $BiVO_4$ photocatalyst: activity enhancement methods for solar photocatalytic applications. *Appl. Catal. A*, 2018, **555**, 47–74.
14. Ran, J. *et al.*, Immobilizing CuO/$BiVO_4$ nanocomposite on PDA-templated cotton fabric for visible light photocatalysis, antimicrobial activity and UV protection. *Appl. Surf. Sci*., 2019, **493**, 1167–1176.
15. Akhtar, M. A., Sharma, V., Biswas, S. and Chandra, A., Tuning porous nanostructures of $MnCo_2O_4$ for application in supercapacitors and catalysis. *RSC Adv*., 2016, **6**, 96296–96305.
16. Lei, B. X., Zhang, P., Wang, S. N., Li, Y., Huang, G. L. and Sun, Z. F., Additive-free hydrothermal synthesis of novel bismuth vanadium oxide dendritic structures as highly efficient visible-light photocatalysts. *Mater. Sci. Semicond. Proc.*, 2015, **30**, 429–434.
17. Velmurugan, M. and Chen, S. M., Synthesis and characterization of porous $MnCo_2O_4$ for electrochemical determination of cadmium ions in water samples. *Sci. Rep*., 2017, **7**, 1–8.
18. Sontakke, S., Modak, J. and Madras, G., Effect of inorganic ions, H_2O_2 and pH on the photocatalytic inactivation of *Escherichia coli* with silver impregnated combustion synthesized TiO_2 catalyst. *Appl. Catal. B*, 2011, **106**, 453–459.
19. Sontakke, S., Modak, J. and Madras, G., Photocatalytic inactivation of *Escherischia coli* and *Pichia pastoris* with combustion synthesized titanium dioxide. *Chem. Eng. J*., 2010, **165**, 225–233.
20. Technical Resources in Biotechnology (internet). Bio-Resource; 2019; http://technologyinscience.blogspot.com/2011/11/cfu-colony-forming-unit-calculation.html#.X-mnaVUzbIX (accessed on 6 August 2019).
21. How to Calculate CFU from Dilution (internet). Sciencing, 2019; https://sciencing.com/cfu-microbiology-15601.html (accessed on 6 August 2019).
22. Wang, Z. *et al*., $BiVO_4$ nano-leaves: mild synthesis and improved photocatalytic activity for O_2 production under visible light irradiation. *CrystEngComm*, 2011, **13**, 2500–2504.
23. Hao, X., Liu, X., Chen, Y., Li, X. and Zhao, Y., The synergic effects of light harvesting and separation of charge carriers, and the optimal band gap of photocatalysts by investigating $Bi_8V_2O_{17}$, $Bi_4V_2O_{11}$, $BiVO_4$ and $Bi_4V_6O_{21}$. *Chem. Phys. Lett*., 2022, **787**, 139154.
24. Sunny, A. and Prabu, N. M., Enhancement of photocatalytic activity of $BiVO_4$ by barium doping. *Indian J. Chem. A*, 2020, **59**, 775–782.
25. Lin, L., Su, Z., Li, Y. and Zhang, C., Comparative performance and mechanism of bacterial inactivation induced by metal-free modified g-C_3N_4 under visible light: *Escherichia coli* versus *Staphylococcus aureus*. *Chemosphere*, 2021, **265**, 129060.
26. Zeng, X. *et al*., Cooperatively modulating reactive oxygen species generation and bacteriaphotocatalyst contact over graphitic carbon nitride by polyethylenimine for rapid water disinfection. *Appl. Catal. B*, 2020, **274**, 119095.
27. Zhang, G., Zhang, Z., Xia, D., Qu, Y. and Wang, W., Solar driven self-sustainable photoelectrochemical bacteria inactivation in scale-up reactor utilizing large-scale fabricable Ti/MoS_2/MoO_x photoanode. *J. Hazard. Mater*., 2020, **392**, 122292.
28. Pingmuang, K., Chen, J., Nattestad, A., Kangwansupamonkon, W. and Phanichphant, S., Photocatalytic degradation of methylene blue by innovative $BiVO_4$/TiO_2 composite films under visible light irradiation. *J. Environ. Sci*., 2014, **3**, 69–76.
29. Su, J., Guo, L., Bao, N. and Grimes, C. A., Nanostructured WO_3/$BiVO_4$ heterojunction films for efficient photoelectrochemical water splitting. *Nano Lett.*, 2011, **11**, 1928–1933.
30. Li, Y., Wu, M. S. and Ouyang, C. Y., The structural and electronic properties of spinel $MnCo_2O_4$ bulk and low-index surfaces: from first principles studies. *Appl. Surf. Sci*., 2015, **349**, 510–515.
31. Zheng, J. and Zhang, L., Incorporation of CoO nanoparticles in 3D marigold flower-like hierarchical architecture $MnCo_2O_4$ for highly boosting solar light photo-oxidation and reduction ability. *Appl. Catal. B*, 2018, **237**, 1–8.
32. Xin, Q. *et al*., Antibacterial carbon-based nanomaterials. *Adv. Mater*., 2019, **31**, 1804838.
33. Adán, C., Marugán, J., Obregón, S. and Colón, G., Photocatalytic activity of bismuth vanadates under UV-A and visible light irradiation: inactivation of *Escherichia coli* vs oxidation of methanol. *Catal. Today*, 2015, **240**, 93–99.
34. Jayaraman, T., Raja, S. A., Priya, A., Jagannathan, M. and Ashokkumar, M., Synthesis of visible-light active V_2O_5/g–C_3N_4 heterojunction as an efficient photocatalytic and photoelectrochemical performance. *New J. Chem.*, 2015, **39**, 1367–1374.
35. Bavani, T., Madhavan, J., Prasad, S., Al Salhi, M. S. and AL Jaffreh, M., A straightforward synthesis of visible light driven $BiFeO_3$/$AgVO_3$ nanocomposites with improved photocatalytic activity. *Environ. Pollut.*, 2021, **269**, 116067.

ACKNOWLEDGEMENT. We thank M.S. Ramaiah University of Applied Sciences and R.V. College of Engineering, Bengaluru for support to carry out this work.

Received 10 January 2022; revised accepted 6 October 2022

doi: 10.18520/cs/v124/i2/183-189